A new parameter to empirically describe and predict the non-linear seismic response of sites derived from the analysis of Kik-Net database

David Castro-Cruz, Julie Regnier, Etienne Bertrand, Françoise Courboulex

A new parameter to empirically describe and predict the non-linear seismic response of sites derived from the analysis of Kik-Net database

Authors

David Castro-Cruz[a,b,*], Julie Régnier[a], Etienne Bertrand[a], Françoise Courboulex[b]

[a] CEREMA, Agence de Sophia Antipolis, 06903 Valbonne, France

[b] Université Côte d'Azur, CNRS, Observatoire de la Côte d'Azur, IRD, Géoazur, 06560 Valbonne, France

Email addresses:

david.castro@cerema.fr (D. Castro-Cruz) , julie.regnier@cerema.fr (J. Régnier), etienne.bertrand@cerema.fr (E. Bertrand), courboulex@geoazur.unice.fr (F. Courboulex)

Corresponding author: David Castro-Cruz

Abstract

We evaluate the non-linear site response at the stations of the Japanese Kik-Net network by computing the ratio between the Fourier spectra of the recordings at the surface and at the downhole station. When the amplitude of the input signal increases, we observe a shift of the resonance peaks towards lower frequencies, characteristic of non-linear soil behavior. We propose a new parameter called *fsp* to characterize this shift. We observe that *fsp* is a good proxy for the shear modulus reduction by comparing *fsp* and the modulus reduction curve obtain by both laboratory test measurements and numerical approaches. The *fsp* is used to correct the linear site response and surface ground motion in frequency domain in order to take into account the non-linear soil behavior. We show that the procedure we established reduces the error in predicting the main frequency peak by 50% compared to an elastic evaluation of the site response during the 2016 Kumamoto earthquake (Mw=7.1).

Keywords: Non-linear site behavior; site effect; Kik-net; Ground motion prediction; Kumamoto Earthquake

Highlights:

- Quantification of non-linear site effects during a ground motion.
- Quantification of the propensity of a site to develop non-linear site effects.
- Prediction of strong motion during the Kumamoto 2016 (Mw 7.1) earthquake.
- A parameter based on borehole recordings to quantify non-linear site behavior.

Funding: This research has been funded by a PhD Grant and work environment from CEREMA.

1 Introduction

It is widely recognized that soft soils can amplify dramatically the seismic motion compared to rock reference site because of seismic waves being trapped in sub-surface sedimentary layers [1–3]. The seismic site response depends on the site geometric configuration, the nature of the soil and the incoming ground motion [4]. For weak ground motion, the combination of a complex site configuration and various incident wave field induces a variability on the site response [5]. For strongest ground motions, the soil non-linear behavior can, in addition, have a strong influence on the site response [6,7]. An accurate prediction of strong ground motion on sedimentary site will, therefore, require the consideration of non-linear soil behavior.

In laboratories, under cyclic and seismic loading, the soil non-linear behavior is illustrated in terms of hysteretic loops in the stress-strain plan [8,9]. The effects of non-linearity in the soil mechanical behavior are generally a reduction of the shear modulus with increasing strain and an increase of the dissipation of energy within the material. Consequently, the hysteretic behavior of the soil can be recovered knowing the shear modulus reduction curve (G/G_{max}) and the damping (ξ) curves .

For the transfer function, that quantify the site response, the effects of the non-linear soil behavior leads in a shift of the resonance frequencies of the site towards lower frequency, induced by a decrease of the apparent shear wave velocity, associated in most of the cases to an attenuation of the high frequency amplifications [10]. Nevertheless, an increase of the amplification at high frequency has been also sometimes reported, which was associated with a decrease of the pore water pressure when cyclic mobility occurs [11] or soil hardening [12]. Many studies show that these differences are larger when the intensity of the incident motion increases (e.g. [13–15]).

The non-linear soil parameters can be characterized by various methods from laboratory testing on soil samples to lower cost method based on correlations between non-linear parameters and other soil parameters (e.g. [16,17]). In-situ measurements can also be used in addition to laboratory tests to infer these non-linear parameters. Some authors use accelerometric data to determine the shear modulus reduction and damping curves. These parameters are often estimated by finding the best numerical model that reproduces the accelerometric time histories. It has been applied mainly in Taiwan and in Japan (e.g. [18–20]). Other authors use interferometry between recordings at different depth to derive the instantaneous wave propagation velocity in the media depending on the input motion intensity [21,22].

Another way to study soil non-linear behavior is to compare site-response curves computed from weak motion and strong motion. In Noguchi and Sasatani [23] the ratio between the Fourier spectrum of records at the surface and at downhole (*BSR*) are computed. They compared *BSR* from weak and strong ground motion by the summation of the differences at each frequency between each *BSR*, parameter that was called DNL (Degree of Non-linearity). They showed a link between the nonlinear effects (defined as DNL), and an intensity parameter of the shaking (PGA). In Lussou et al. [24] and Régnier et al. [7], several parameters are proposed to quantify those differences, such as an estimation of the modification of the *BSR* curves and a measurement of the frequency shift. In Field et al. [25] ratios between spectral ratios were computed using synthetic rock reference seismograms. Similarly, in Régnier et al. [10] the ratio of the non-linear to linear spectral ratios are analyzed, but using vertical arrays. In all cases, the authors found that the non-linear to linear site response discrepancy is related to the frequency range and increase with increasing PGA of the incident ground motion.

Following a similar approach, we compare weak motion and strong motion site responses in order to propose a methodology for correcting the linear site response in order to reproduce the effects of non-linear soil behavior based on the analysis of recordings from vertical arrays of the Japanese Kiban Kyoshin network (KiK-Net). After a description of our approach, an application will be detailed on the recordings of the 2016 Kumamoto Japanese earthquake.

2 Data

To study the influence of the non-linearity of the soil behavior on the empirical *BSR*, we use the KiK-net dataset in Japan. These data are available on the web page of the National Research Institute for Earth Science and Disaster Prevention (http://www.kyoshin.bosai.go.jp). The network is composed of 688 stations, among them, 650 sites are characterized with *Vs* and *Vp* profiles, soil description, and information on the stations (location and information of recording devices). For each recorded earthquake, the acceleration time histories are provided, with the event origin time, the epicenter location, the depth of the hypocenter, and the magnitude of the earthquake determined by the Japanese Meteorological Agency.

We selected recordings according to two criteria: signals from earthquakes with a magnitude higher than 3 and with an epicentral distance lower than 500 km. Under those two criteria, we use 75 232 signals (each one recorded in the three directions at the surface and at downhole) from 5 535 earthquakes with magnitudes between 3 and 9, recorded between November 1997 to December 2017. Figure 1 presents the whole selected records used in our analysis.

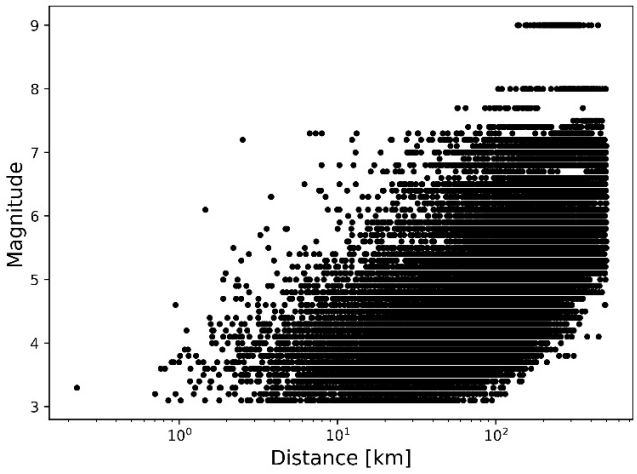

Figure 1. Magnitude/distance distribution of earthquakes recordings used in this study.

Subsequently, for all of the selected seismograms a signal processing based on Boore [26] recommendations was applied. It consists in: (1) removing the mean, (2) removing the data before the first zero-crossing point, (3) Applying an Hanning's window to improve the trimming process of the signal [27], and finally (4) Applying two times a high pass filter of 2nd order with fc=0.1 Hz. This processing allows to remove the low-frequency noise and to ensure compatibility between acceleration, velocity and displacement time series and Fourier and response spectra. In particular, effects of spurious low frequency can be removed from the data through this procedure.

The empirical site response is assessed on the horizontal components by computing the Borehole Spectral Ratios (*BSR*), defined as the ratio between the geometric average of the Fourier amplitude spectra of the horizontal components at the surface and at downhole (Equation (1)).

$$BSR(f) = \sqrt{\frac{EW_{surf}^2 + NS_{surf}^2}{EW_{depth}^2 + NS_{depth}^2}} \quad \textbf{(1)}$$

Where *EW* and *NS* are the amplitude of the Fourier transform of the accelerograms for East-West, and North-south horizontal components respectively. In this study, we applied a Konno-Ohmachi smoothing [28] to each spectrum, improving the comparison between spectra and avoiding zero values at the denominator of

(Equation (1)). *BSR* shows, in the frequency domain, how the seismic signal varies between the downhole sensor and the one at the surface. *BSR* curves indicate the site resonance frequencies $f^{(n)}$ if the downhole sensor is located at the main sediment to substratum interface. Otherwise, the curve includes pseudo-resonances that are induced by the destructive interferences of the down-going waves with the incident ones at the downhole sensor [29]. However, the comparison of weak and strong site response remains relevant to characterize non-linear site behavior.

3 Method

Our method defines a parameter called *fsp* that characterize the non-linear site behavior. To illustrate our methodology, we detail the whole procedure on one site of the KiK-net database (IBRH11) that has recorded both weak and strong ground motions. Then, we compare the parameter *fsp* to laboratory data (shear modulus reduction curves) obtained from cyclic tri-axial test at one Kik-net site (KSRH10), that was characterized during a previous PRENOLIN project [30]. Finally, the parameter is tested analytically by using non-linear site response calculations on simple site configuration (1-D, non-linear, mono-layer cases).

3.1 *fsp*: a new parameter to characterize non-linear site behavior

In order to explain our methodology, we detail the whole method on one site of the KiK-net database that has recorded a large panel of earthquakes from weak to strong motions. Then, we will generalize the procedure to all of the stations. Station IBRH11 has recorded 515 earthquakes and it is located in the prefecture of Ibaraki (Figure 2) on a D-site according to the Eurocode 8 (EC8) with a Vs_{30} of *242 m/s* ($Vs_{30} = {}^{30}/_{\sum h_i/Vs_i}$) and a depth of 103 meters. The bedrock is reached at 30m depth and is characterized with a Vs of 2100 m/s. The downhole station is situated at 100m depth.

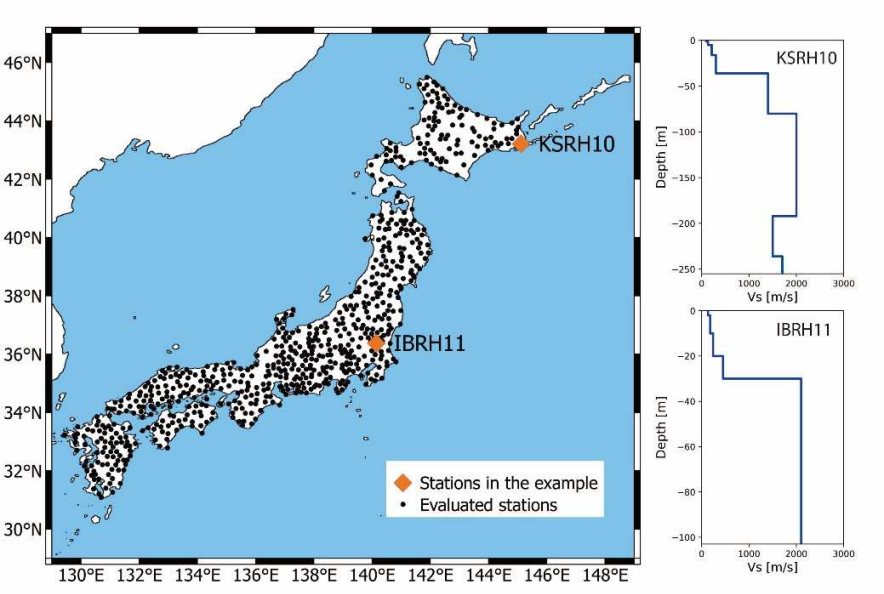

Figure 2. Location and Vs profiles of stations IBRH11 and KSRH10 and the other stations (Japanese Kik-net network).

Figure 3 illustrates four *BSR* computed at IBRH11 from ground motions with different levels ($PGA_{downhole}$). We observe that weak ground motions share a similar *BSR*. This is because for weak ground motion the site response is linear [13]. The variability that can still be observed in the site response for these small seismic solicitations is mainly due to complex site geometry associated to the distribution of earthquake sources

around the site [5]. For stronger ground motions, the peak frequencies occur at a lower frequency bandwidth. We interpret this shift as a direct effect of the shear modulus reduction of the soil when the seismic solicitation increases. Furthermore, the decrease in the amplitude of *BSR* is another effect of non-linear soil behavior linked to the increase of damping with shear strain, but in the following we will only discuss about the frequency shift impact.

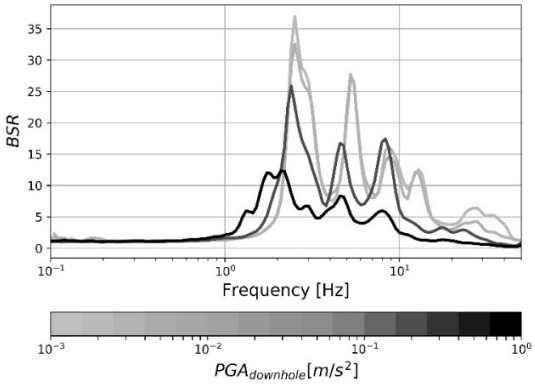

Figure 3. *BSR* at IBRH11 station (KiK-net) for four earthquakes with different PGA at the downhole station.

The weak ground motions for which the site behaves linearly are selected based on their maximal peak accelerations. Indeed, the ground motions with a $PGA_{downhole}$ from 10^{-4} m/s^2 to $6.\ 10^{-3}$ m/s^2 are considered. Figure 4 presents the BSR_{linear} with a dotted line. It is the arithmetic average of all of the weak ground motions *BSR* (grey curves). The black line represents the *BSR* computed from a strong ground motion with $PGA_{downhole}$ of 2.6 m/s^2. It is easy to appreciate that the resonance peaks of the *BSR* from this strong ground motion are shifted to lower frequencies and that their amplitude are the smallest.

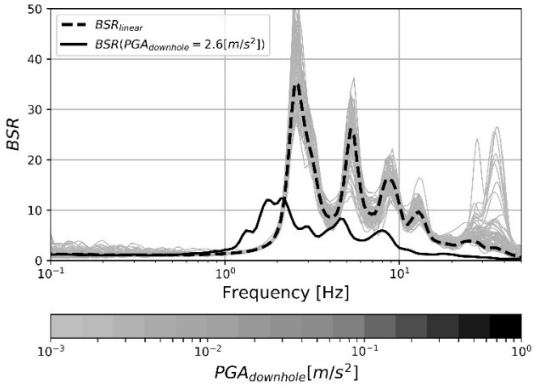

Figure 4. Definition of BSR_{linear} as the average of all of the weak ground motions (142 events) and comparison between BSR_{linear} with the *BSR* computed from one strong ground motion.

BSR_{linear} is compared to each *BSR* from all of the recorded ground motions, allowing us to define a parameter that characterizes the observed frequency shift. The logarithmic frequency shift is the gap in logarithmic scale between BSR_{linear} and *BSR*. In linear scale, it is a coefficient that changes the frequency scale. The algorithm to find this logarithmic shift minimizes the misfit between BSR_{linear} and *BSR* as defined in the Equation (2). Note that the misfit is weighted by the logarithmic sampling.

$$misfit = \sum_i \left| BSR_{linear}\left(\bar{f}/_{Ls}\right) - BSR(\bar{f}) \right| \Delta x$$
$$\Delta x = log_{10}(f_{i+1}/f_i) \quad and \quad \bar{f} = 0.5 \cdot (f_{i+1} + f_i) \qquad \textbf{(2)}$$

In the Equation (2) *Ls* is the logarithmic shift applied to BSR_{linear}. The *misfit* is defined as a discrete approximation of the area between the shifted BSR_{linear} and *BSR*, considering a logarithmic scale as the length of the base (*Δx*). The computation is done over a frequency window going from 0.3 Hz to 30 Hz.

Finally, we define a frequency shift parameter, so called *fsp,* as the square of the *Ls,* which produces the minimum value of misfit (*fsp=Ls² when misfit is minimized*). The *fsp* is a coefficient that is applied to the linear resonance frequency to obtain the non-linear ones for a specific ground motion. It means that if no shift is needed to fit both curves, both *Ls* and *fsp* are equal to one. If BSR_{linear} needs to be logarithmically shifted to higher frequencies to fit *BSR*, *fsp* will be higher than one. In the opposite case, *fsp* will be lower than one. Non-linear soil behavior is expected to shift the *BSR* to lower frequency range and therefore linked to an *fsp* below one.

fsp is computed for every recording collected at station IBRH11. The results (Figure 5) shows the evolution of *fsp* in function of the ground motion intensity, expressed in terms of the *PGA* recorded at the downhole station. For small *PGA*, *fsp* is close to *1*, but as the solicitation level increases, the value starts to decrease. The decrease is gentle for *PGA* smaller than *0.1 m/s²* but is growing rapidly for larger seismic solicitations. A hyperbolic curve is used to fit the *fsp* values (Equation (3)), with a formulation equivalent to the one used to describe the modulus reduction curves [31,32].

$$fsp = \frac{1}{1+\frac{\mathrm{PGA_{downhole}}}{\mathrm{PGA_{Refdownhole}}}} \qquad \textbf{(3)}$$

Where $PGA_{Ref_{downhole}}$ is a parameter that describes the hyperbolic function for each site. It is equal to the $PGA_{downhole}$ corresponding to *fsp=0.5*, this parameter being the counterpart of γ_{ref} in the hyperbolic models and the only parameter that is needed to fully describe the hyperbolic function. In order to quantify the variability of *fsp*, a single standard deviation is computed for each station considering the whole number of data. The dashed lines on Figure 5 represents the mean plus or minus one standard deviation.

Here, $PGA_{downhole}$ can be considered as an estimator of the strain level that the site can experience during each earthquake. Others proxy of strains have already been proposed in the literature. For example, Chandra [33] proposed PGV/VS_{30} as a strain proxy. We decided to use first the *PGA* recorded at the downhole station instead because the integration from acceleration to velocity may add some uncertainties in the *PGV* calculation. Also *PGA* is a relevant parameter for describing the amount of non-linearity a soil may produce [7].

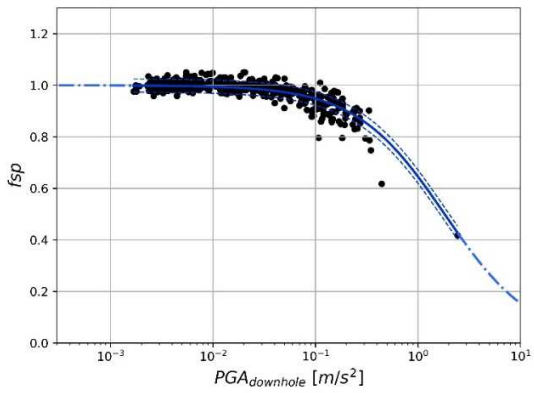

Figure 5. *fsp* value against PGA at downhole (*fsp* curves). Black line best hyperbolic function that fits the data. Station IBRH11 - VS_{30}: 242 m/s.

3.2 *fsp* parameter compared to the shear modulus reduction curves

We compute the *fsp* parameter for the earthquakes recorded at station KSRH10. This site is situated in the Hokkaido prefecture, has recorded 283 events, and is located on a D-site according to EC8 (Vs_{30} of *212 m/s).* This station is particularly interesting because it has been well characterized by in-situ and laboratory data measurements performed during the PRENOLIN project [30]. We plot the *fsp* values computed for this site against the *PGV* at the surface divided by Vs_{30}, as a proxy for strain, to compare with the shear modulus reduction curves obtain from cyclic tri-axial tests performed at this station (Figure 5). We observe that the *fsp* values are in the range of the shear modulus reduction curves. From this comparison we are convinced that *fsp* is a good proxy for the shear modulus reduction with shear strain.

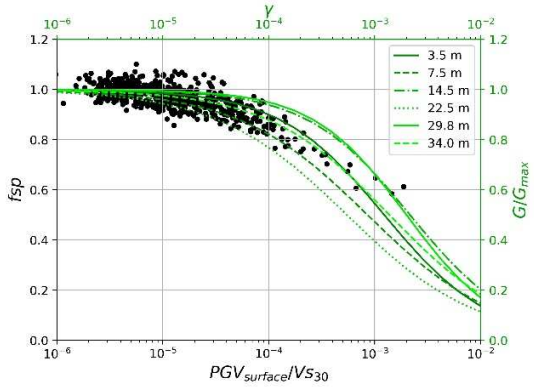

Figure 6: Shear modulus reduction curves defined in the PRENOLIN project at station KSRH10 (green lines) at different depths from cyclic triaxial tests and *fsp* against PGV/ Vs_{30} calculated at the site. The color version of this figure is available only in the electronic edition.

3.3 Comparison with analytical and numerical modeling

We also test *fsp* analytically and with numerical modeling. First, we analyze the *fsp* analytically in a very simple case and then we apply our calculations to a more complex wave propagation in truly non-linear soil model.

In linear domain with 1-D configuration of a mono-layer soil and considering vertical incidence of the shear waves, the resonance frequencies ($f^{\{n\}}$) depend on the shear velocity (*Vs*) and the layer thickness (*H*) through $f^{\{n\}}$=*Vs(1+2n)/(4H)*. The shear velocity (V_s) can be expressed as a function of the shear modulus as $v_s = \sqrt{G/\rho}$ where *G* and *ρ* are the shear modulus and the density respectively. The shear modulus of the layer can thus be derived knowing the associated resonance frequencies using the Equation (4).

$$G = \left({2 \cdot H \cdot f^{\{n\}}} \Big/ {(0.5 + n)} \right)^2 \rho \qquad \textbf{(4)}$$

In the equivalent linear approximation (EQL), the nonlinearity of the soil behavior is taken into account in an iterative process that adjusts the elastic properties to the level of strain induced in the layer, knowing both the modulus reduction and the attenuation curves. In this frame, the shear modulus at a linear strain rate (G_{max}) can be compared to the shear modulus at larger strain (*G*), by the ratio between both. Using the Equation (4) for both modulus, the ratio will be expressed as followed:

$$\frac{G}{G_{max}} = \left({f^{\{n\}}}/{f^{\{n\}}_{linear}} \right)^2 = fsp \quad \textbf{(5)}$$

The Equation (5) shows that the ratio of the shear modulus is proportional to the square root of the ratio between the linear resonance frequency f_{linear} and the non-linear ones (whatever the order of the harmonic). In logarithmic scale, this ratio (f/f_{linear}) represents a logarithmic shift, and this shift can be found minimizing the Equation (2). Computing the square of the logarithmic shift that minimizes the Equation (2) is, once again, the definition of the *fsp* parameter. Therefore, in this very simple case, the shear modulus reduction is equal to the previously defined *fsp*.

In a fully non-linear model, it is not possible to derive an analytical formulation as for the equivalent linear approach. Therefore, the relationship between the shear module reduction with strain increase and the shift of the resonance frequencies towards lower frequencies must be analyzed using numerical simulation and numerical *BSR* calculation. To simulate the seismic response, we are using a 1-D fully non-linear approach implemented in CyberQuake software proposed by Modaressi et al. [34] and based on a plastic constitutive model with hardening based elastoplastic theory [35]. We compare the results to the ones computed with an equivalent linear model also implemented in CyberQuake. We are considering a model composed of a single layer of 40 m of thickness with a shear wave velocity of 200 m/s over an elastic bedrock. In the linear domain, the fundamental resonance frequency of this soil column is equal to 1.25 Hz. For the EQL, the non-linear properties are homogeneous along the depth and illustrated in Figure 7. For the fully non-linear approach, the soil mechanical parameters are also shown in Figure 7. Those parameters were chosen as they characterize a typical non-linear soil layer [36]. The non-linear constitutive model implemented defines non-linear properties that depends on the confining pressure and consequently on the considered depth, while Vs remains the same in the whole layer. Figure 7 shows in green the modulus reduction curves and damping curves at different depths.

The bedrock is modeled as an infinite monotonic and elastic material with shear velocity of *1500 m/s*, a density of *2000 kg/m³*, and a Poisson coefficient of 0.3. A Gabor wavelet is used as input signal. This simple wavelet makes easier the evaluation of non-linear effects in the *BSR*. The Gabor's wavelet is defined with the Equation (6).

$$F(t) = Ae^{-\left(\frac{2\pi f_m(t-to)}{\gamma}\right)^2} cos(2\pi f_m(t-to)) \quad \textbf{(6)}$$

In the simulations, γ is taken as 3, t_o as *2.5s*. The central frequency (f_m*=1.25 Hz*) is chosen in agreement with the fundamental resonance frequency of the site and only frequencies lower than *2 Hz* are analyzed, as the

energy of the input signal at higher frequencies is too small to make the ratio computation relevant. *A* corresponds to the maximal amplitude of the signal.

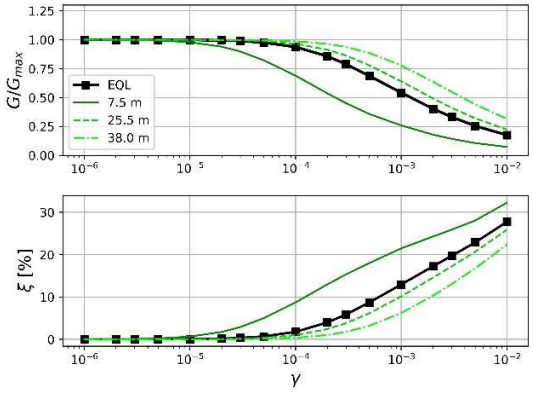

Figure 7. Modulus reduction curve and damping curve that are used in: Equivalent Linear approx. (black line-squares), and at different depths for the full non-linear model (green lines). The color version of this figure is available only in the electronic edition.

For the fully non-linear approach, the soil mechanical parameters are given in Table 1. They were chosen as they characterize a typical non-linear soil layer [36]. In the linear domain, the fundamental resonance frequency of this soil column is equal to 1.25 Hz.

Table 1. Parameters of the soil layer for the 1-D numerical simulation.

Vs[1] (m/s)	200
Vp[2] (m/s)	374
ρ[3] (Kg/m³)	1750
Φ[4](°)	25
β[5]	10
σ_{ci}/σ_v[6]	2
Ep[7]	20
C[8] (kPa)	0
$\gamma_{elastic}$[9]	$1x10^{-9}$
b[10]	0.9
nr[11]	0.4
ψ[12](°)	20

[1] Shear wave velocity (m/s)
[2] Primary wave velocity (m/s)
[3] Density (Kg/m³)
[4] Friction angle at totally mobilized plasticity (°)
[5] Plastic modulus
[6] Compaction ratio
[7] Plastic stiffness coefficient
[8] Cohesion (kPa)
[9] Extent of the truly elastic domain
[10] Shape parameter of the yield Surface
[11] Numerical parameter of isotropic hardening
[12] Slope of the characteristic line (°)

α_ψ[13]	0.8

We test different input signal amplitudes and calculate the *BSR* in each case. The maximum amplitudes of the signals are: 0.001, 0.01, 0.05, 0.1, 0.3, 0.7 and 1 m/s^2, results are shown in Figure 8. For the smallest PGA, the computed *BSR* is equivalent to the analytical elastic case (black dash line). As expected for the larger input motions, the amplification peak is smaller, and it is shifted towards lower frequencies. The equivalent linear computation (Figure 8A) leads to resonance frequency shift larger than the fully non-linear approach (Figure 8B). Indeed, besides the limitations of EQL approaches at large strain [37], the non-linear soil properties differ in the two numerical approaches as mentioned above. Indeed, at the soil to bedrock interface, the non-linear soil properties are much more linear in the fully non-linear computation.

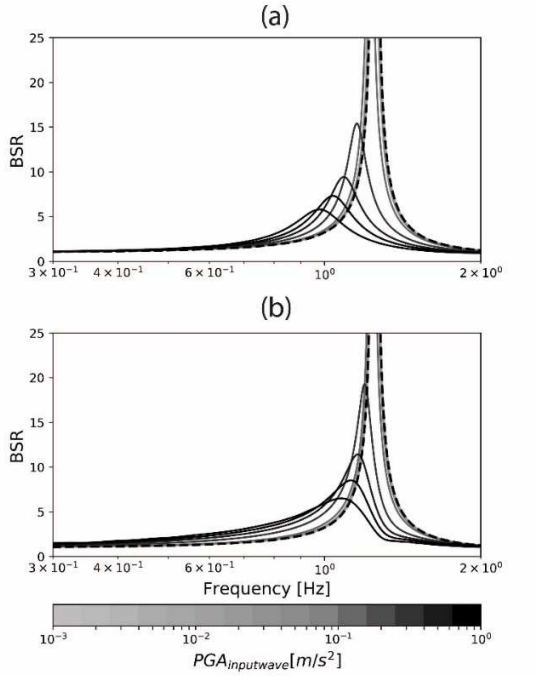

Figure 8. *BSR* for the equivalent linear approach (a) and the fully non-linear simulation (b) for a different level of input solicitation. Black dash is the elastic response curve.

In the linear equivalent approach, the effective strain (γ_{eff}) is used to calculate the equivalent shear modulus and damping at each iteration. It is defined from the maximal strain as $\gamma_{eff} = 0.65\gamma_{max}$. In Figure 9a, the values of the G/G_{max} ratio computed using γ_{eff} and γ_{max} are compared to the appropriate *fsp* values. Taking into account γ_{max} leads to a misfit between *fsp* and the ratio at high deformation level. Those differences are related to the EQL methodology who computes the non-linear parameters with γ_{eff} instead γ_{max}. Considering G/G_{max} at γ_{eff}, the frequency shift equals almost the shear modulus reduction. The small error can be attributed to the iteration scheme implemented in the linear equivalent method. The good fitting between G/G_{max} and *fsp* curves shows that *fsp* parameter is able to quantify the amount of shear modulus reduction as equivalent linear method does in this very simple mono-layer case.

Figure 9b presents the G/G_{max} ratio at different depths in function of the *fsp* parameter calculated from the *BSR* curves for a full non-linear approach. The G/G_{max} ratio used in these graphs is computed considering the effective strain (γ_{eff}) at the middle of the layer for various depths in the non-linear computations (Figure 7).

[13] Parameter of the magnitude of the dilatancy

From this figure, we observe that G/G_{max} and *fsp* are not equivalent at all depths in the fully non-linear approach. Indeed, the curves showed on the graph depend on the depth considered for the computation of the shear modulus, as both the non-linear soil properties and the shear strain varies with depth. However, we notice that Equation (5) still can be applied to the curve computed at 25.5 m at depth. At this specific depth, the reason why *fsp* is not perfectly equal to the G/G_{max} ratio on the whole *fsp* range could be related to the definition of γ_{eff} using an approximation of the shear strain during the shaking. At shallower depths, *fsp* overestimates the shear modulus decrease. On the contrary, at larger depths *fsp* underestimates slightly the G/G_{max} ratio.

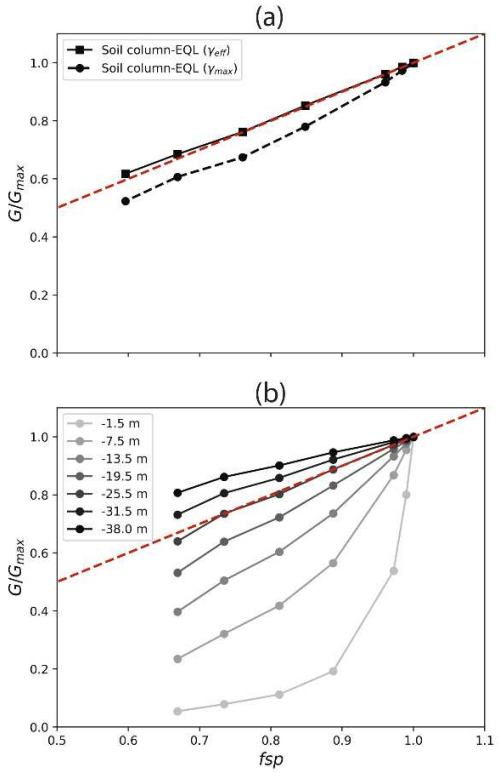

Figure 9. Evolution of the shear decay reduction in function of *fsp*. Left: equivalent linear approach. Right: full non-linear simulation. Red dotted curve: G/G_{max} = *fsp*. The color version of this figure is available only in the electronic edition.

3.4 Prediction of non-linear surface ground motion using *fsp* curves

In order to go further, we aim to develop a methodology to predict the non-linear surface ground motion using the *fsp* curves previously computed. For a given site, knowing the PGA value at the downhole sensor, we propose to estimate *fsp* from the non-linear regression defined in the Equation (3) previously computed at the station. Combining *fsp* and BSR_{linear}, it is possible to estimate the *BSR* for the predicted ground motion. This estimation consists in applying the predicted frequency shift to BSR_{linear} as shown in Equation (7).

$$\widehat{BSR}(f) = BSR_{linear}(f \cdot \sqrt{fsp}) \quad \textbf{(7)}$$

where $\widehat{BSR}$ is the estimated borehole spectral ratio for the strong motion, BSR_{linear} the linear borehole spectral ratio, and *fsp*, the estimated frequency shift from the hyperbolic curve defined for the site (Equation (3)).

We then assume that $\widehat{BSR}$ can be used as a borehole transfer function for the specific considered earthquake. With this assumption, using $\widehat{BSR}$ and the ground motion at downhole it is possible to compute the ground motion at the surface :

$$A_{surface} = \widehat{BSR}(f) \cdot A_{downhole} \quad \textbf{(8)}$$

Where $A_{surface}$ represents the Fourier transform of the accelerogram at the surface, $A_{downhole}$ is the Fourier transform of the accelerogram at downhole, and $\widehat{BSR}$ is the estimated borehole spectral ratio computed with Equation (7).

4 Results

4.1 Application to the whole KiK-net database

We compute the *fsp* curves for the 650 considered sites (Figure 10). In order to take into account only the sites where a reliable *fsp* could be derived, we choose to select the 462 sites having a standard deviation lower than 0.07. On figure 10, the curves are drawn with plain lines in the PGA range covered by the data and are represented with dashed lines in the PGA range where the curve is extrapolated. At some sites, the curve is linear over the whole PGA domain, meaning that there is no shift of frequency no matters the intensity of the ground motion is. In other sites, the decrease of *fsp* starts at low PGA, meaning that even for weak motions a shift of the peak frequencies is significant. The variability of the curves reflects the variability of the non-linear soil behavior at the different sites. The figure shows as well, that for some *PGA* at the downhole, all of the sites are prone to develop non-linear soil behavior. For example, for the evaluated stations in this study, 50% of the stations have an *fsp* lower than *0.8* for a $PGA_{downhole}$ of $4.4x10^{-1}$ m/s^2. 25% have developed a lower value of *fsp* for a $PGA_{downhole}$ of $2.3\ x10^{-1}$ m/s^2, and 75% for $PGA_{downhole}$ of $8.4x10^{-1}$ m/s^2.

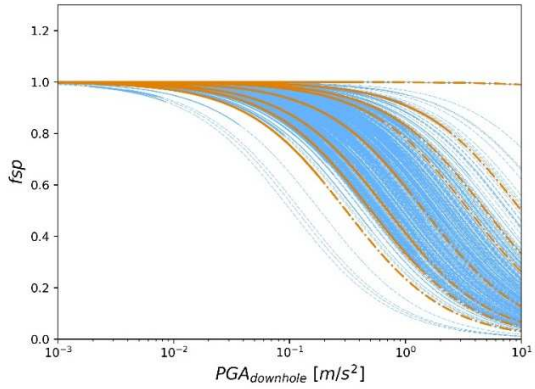

Figure 10. *fsp* curves for 462 sites of the Kik-Net network. Continuous lines indicate that the curves are interpolated using data, dash lines indicate the portion of curves that are extrapolated. Orange line data is shown in Figure 11. The color version of this figure is available only in the electronic edition.

Among all of the KiK-net sites, we performed a selection of 8 sites to show in more details the *fsp* curves. We select sites with different range of $PGAref_{downhole}$ and sites that have recorded very large earthquakes as Fukushima or Kumamoto earthquakes. The *fsp* curves derived at these stations are already shown in orange in Figure 10. They are presented in Figure 11 together with the individual *fsp* obtained for each recorded earthquake. In this figure, the graphs are organized from very non-linear stations to linear ones. The Table 2 shows the $PGAref_{downhole}$, the Vs_{30}, and the depth where the downhole station is located.

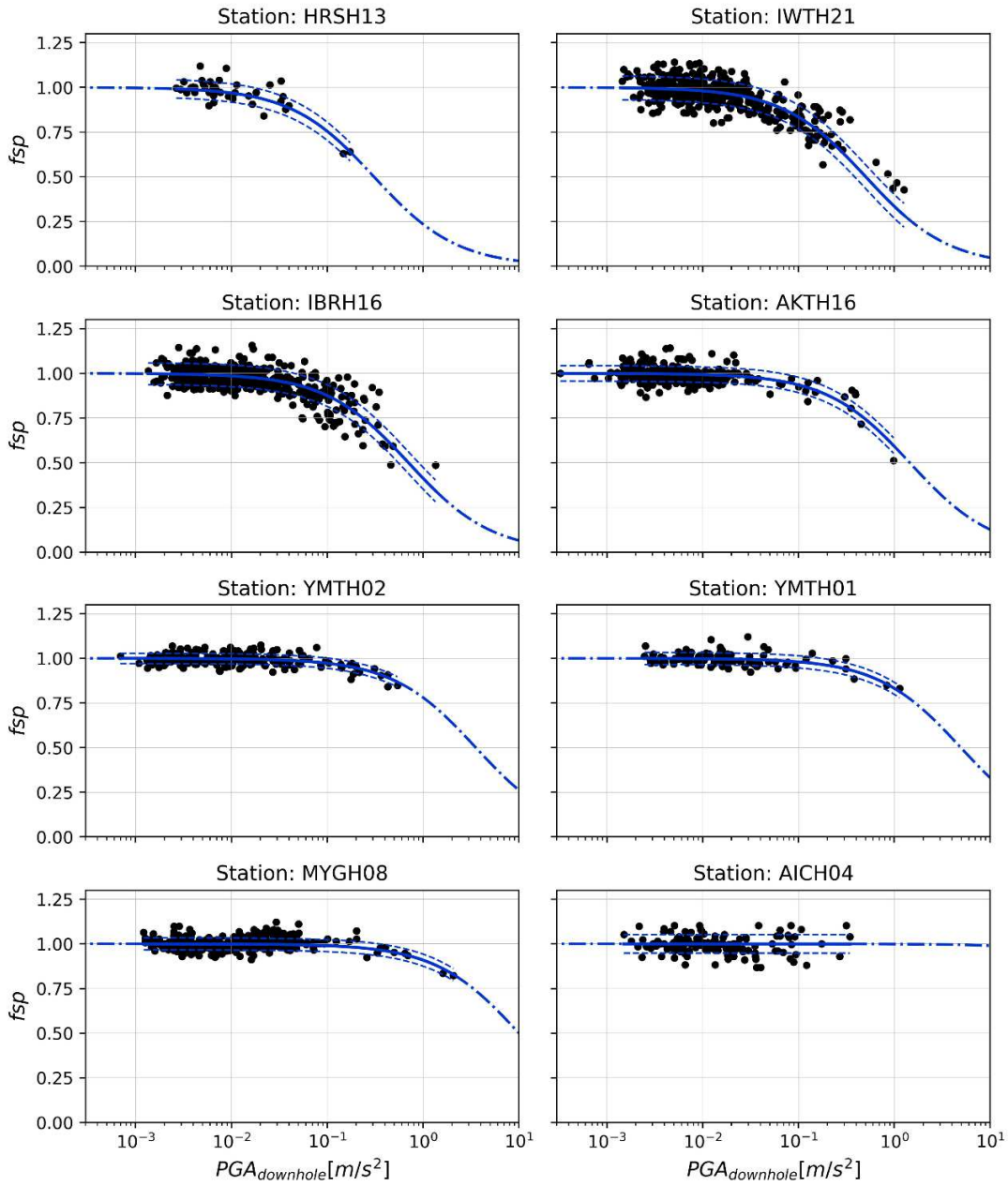

Figure 11. *fsp* curve for several stations that represents the general behavior of the data set. The blue line is the hyperbolic function that is fitted in each case. The color version of this figure is available only in the electronic edition.

Table 2. General data for 10 selected sites.

Station Name	$PGAref_{downhole}$ [m/s^2]	Vs_{30} [m/s]	Depth [m]
HRSH13	3.08E-01	399	200
IWTH21	5.03E-01	521	100
IBRH16	7.05E-01	626	300
AKTH16	1.45E+00	375	154

YMTH02	3.55E+00	279	150
YMTH01	4.95E+00	328	207
MYGH08	1.00E+01	203	100
AICH04	∞	241	1055

PGAref$_{downhole}$ is the parameter that quantifies the susceptibility of a site to show a non-linear behavior. The higher it is, the less non-linear the site is. We can observe that the variation between stations is significant. The *PGAref*$_{downhole}$ go from 3.1x10^{-1} m/s^2 for the station HRSH13 to infinite for AICH04. The hyperbolic trend previously describe is well suited for the *fsp* distribution in function of *PGA*$_{downhole}$ at almost all of the stations. However, we can note that at station IWTH21, the hyperbolic model (blue line) is not necessarily the function that would produce the best fit.

In Table 2, we conclude that the higher Vs30 is, the smaller *PGAref*$_{downhole}$ is, meaning that larger non-linear behavior is observed for site characterized by high Vs30. This has already been reported in previous papers (e.g. Régnier et al., 2014 [7]) with the conclusion that high Vs30 sites, composed of a thin soft soil over a stiff shallow bedrock, create a very large impedance contrast that can induce strong amplification and large strain in the superficial layer during earthquakes.

4.2 Application to 2016 Kumamoto earthquake recordings, Mw 7.1

We apply our methodology to the Kumamoto Earthquake recordings. The earthquake mainshock occurred April 15th, 2016 in the south of Japan (island of Kyushu), with a magnitude Mw of 7.0. This earthquake initially started on a deep portion of the northern part of the Hinagu fault and then finished in the Futagawa fault [38], it was the largest earthquake in Japan in 2016. In this section, the recorded ground motions at KIK-net sites (FKOH03, OITH11, and KMMH03) are compared to predicted ones using the methodology described previously. Figure 12 gives the location of the three sites in the Island of Kyushu, the location of the fault and the epicenter according to Yagi et al., (2016). Station FKOH03 is located at 91 km of the fault located in Umi Fukuoka prefecture, with a Vs_{30} of 497 m/s (site EC8 type C). The bedrock is reached at 25m depth with a Vs of 2030 m/s and the downhole station is located at 100m depth. Station OITH11 is located at 72 km from the epicenter in Kokonoe Oita prefecture. It has been characterized with a Vs_{30} of 458 m/s (site EC8 type C) and the S wave velocity reaches 800 m/s starting from 65m depth, the downhole station is located at 160 m depth with a Vs of 1000m/s. Finally, KMMH03 is located in the prefecture of Kumamoto in Kikuchi at 27.7 km from the epicenter. Like the two other sites, it is a EC8 type C class with a Vs_{30} of 421 m/s. The bedrock was found at 80m with a Vs of 1200 m/s and the downhole station is located at 200m depth where Vs of reaches 2000m/s.

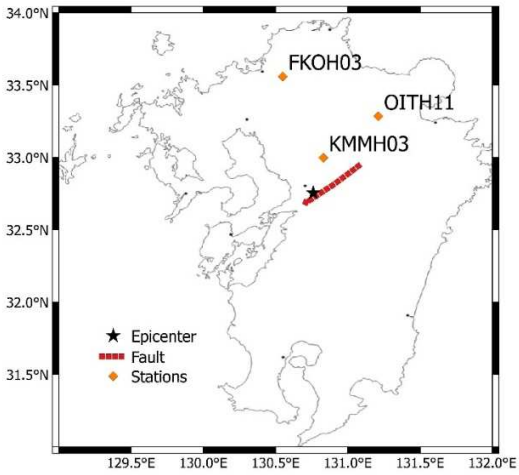

Figure 12. Island of Kyushu Japan with the location of the studied stations. The line and the star represent the location of the active fault and the epicenter for Kumamoto earthquake 15th April 2016 [39].

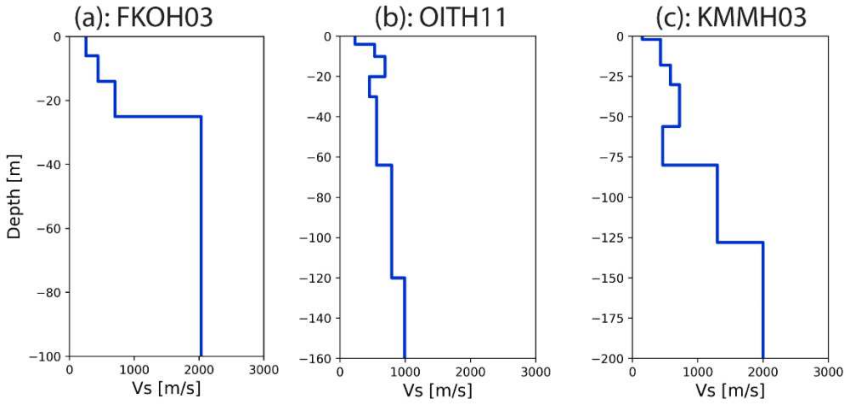

Figure 13. Vs profiles of evaluated sites for the earthquake of Kumamoto 2016. (a) site FKOH03. (b) site OITH11. (c) site KMMH03.

We compute the *fsp* curves for the three sites (Figure 14) using 140, 57, and 111 earthquakes for station FKOH03, OITH11, and KMMH03 respectively leaving on the side the recordings of the main Kumamoto event. On figure 14, we report together with the *fsp* curves, the PGA values at downhole recorded during the Kumamoto earthquake (orange vertical line). We note that the ground motions recorded during this event were larger than all the other events of the database for stations OITH11 and KMMH03. Therefore, for these stations, *fsp* is estimated by extrapolation of the *fsp* curves calculated on weaker motions. The performance of the extrapolation depends on the site and the available data. If no large or medium earthquakes have been recorded at a site, the non-linear regression is not well constrained at larger PGA and the estimated shift will be assorted with important uncertainties. On the contrary, at FKOH03, the *fsp* is assessed by interpolation leading to a better confidence. However, even here, the dispersion between the curve and the real data remains.

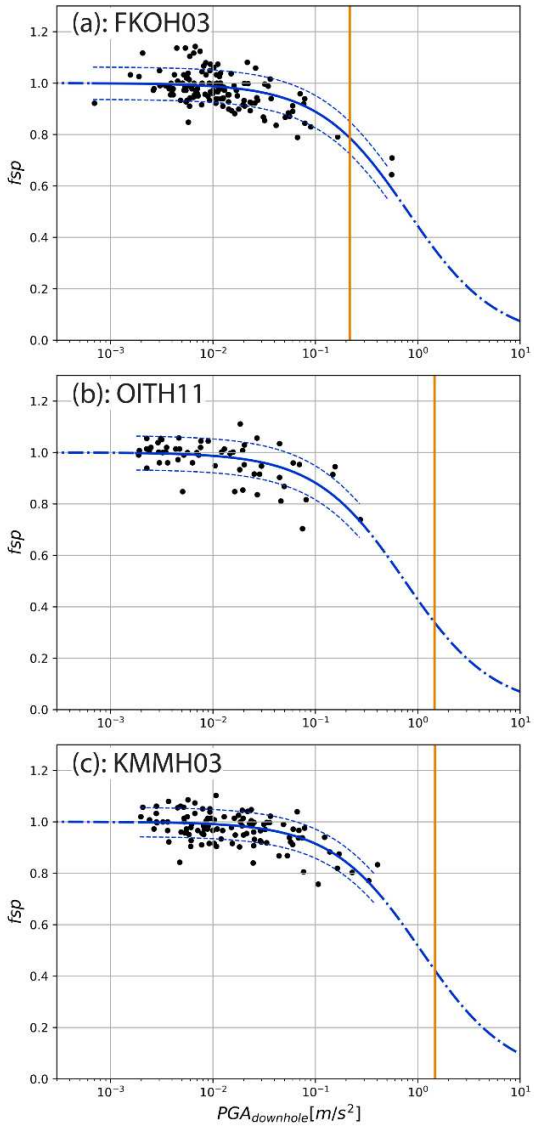

Figure 14. *fsp* parameter in function of the $PGA_{downhole}$. (a) site FKOH03. (b) site OITH11. (c) site KMMH03. The vertical line represents the $PGA_{downhole}$ generated by the Kumamoto 2016 earthquake at each site.

The $\widehat{BSR}$ derived from the BSR_{linear} with the predicted frequency shift are illustrated in Figure 15 in black thick lines along with the observed *BSR* in grey lines and the linear *BSR* in dotted line. For the three cases, the estimated $\widehat{BSR}$ is closer to the observed *BSR* than to the linear *BSR*. This result shows that the shift correction we propose is relevant for large ground motions, when the nonlinear soil behavior is running. Furthermore, we observe that the shift in the *BSR* is well predicted even with an extrapolated *fsp*.

At station FKOH03 that experienced the weaker motion during this earthquake ($PGA_{downhole}$ ~ 0.2 m/s^2), the correction on BSR_{linear} is very small and do not particularly change the frequency content of the motion. But at station OITH11, that recorded a larger $PGA_{downhole}$ (about 2m/s^2), the correction is important leading in a prediction fiting very well the real surface data. On this station, the *BSR* has one main peak and a simple shape. Station KMMH03 also recorded a strong $PGA_{downhole}$ but its *BSR* is more complex, with various peak frequencies (mainly two around 1Hz and 10Hz) over a large frequency band. This station is located within few kilometers

of the active fault. Consequently, it is subject to near-source high frequency effects. The correction applied is very efficient on the lower frequency of the *BSR* but tends to shift a little too much the higher frequency part (> 10z). For this station, we observe that the *s*hift shouldn't be the same for all frequencies. This could be due to others causes than the non-linear soil behavior alone.

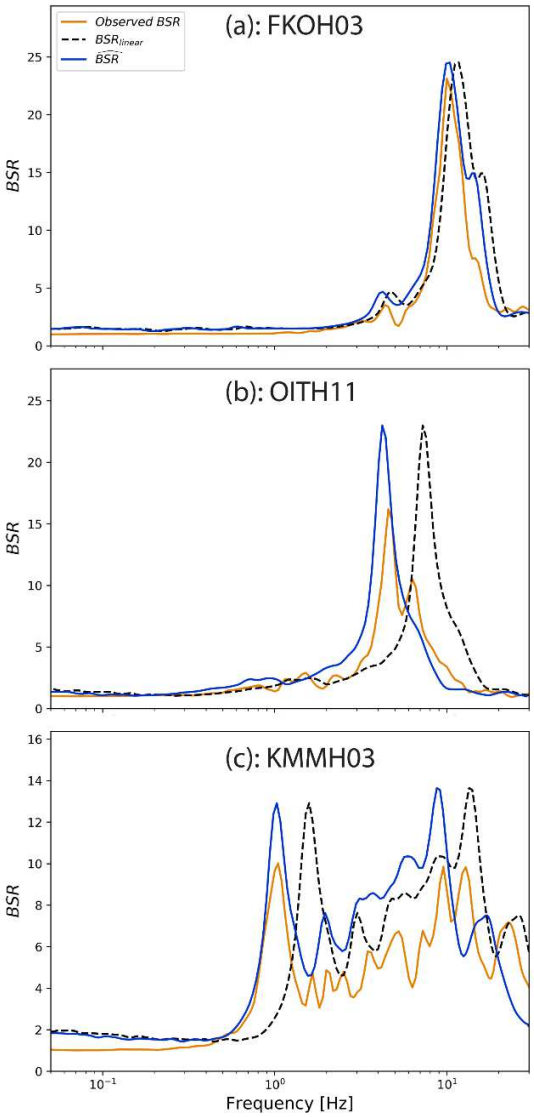

Figure 15. Comparison between the BSR_{linear} for each site (black dashed line) computed on weak motion, the *BSR* computed on the Kumamoto earthquake recordings (orange line), and the correction of the borehole transfer function ($\widehat{BSR}$) that we propose (dark blue line). (a) site FKOH03. (b) site OITH11. (c) site KMMH03. The color version of this figure is available only in the electronic edition.

Table 3 illustrates the improvement offered by the proposed methodology in the predicting of strong ground motion. We compute the difference in frequency of the *BSR* peaks between the observation and the related prediction. From this table, it is clear that the differences are lower when the *BSR* is corrected by the *fsp* shift. Indeed, at OITH11 and KMMH03, the methodology improves the prediction of the frequency peak by around

50%. At FKOH03, the ground motion was not strong enough to show some non-linear soil behavior during the main event. However, even in this case, we can see that a little improvement is provided by our approach.

Table 3. Relative comparison between the main peak frequencies in the observed *BSR, the estimated BSR,* and BSR_{linear}.

	FKOH03	OITH11	KMMH03
$BSR_{Observed}$ to $\widehat{BSR}$	2%	8%	2%
$BSR_{Observed}$ to BSR_{linear}	15%	58%	50%

The Fourier spectrum for the geometric average of the horizontal components is computed according to the Equation (1). The results are presented in Figure 16 for the three sites on which we are focusing here.

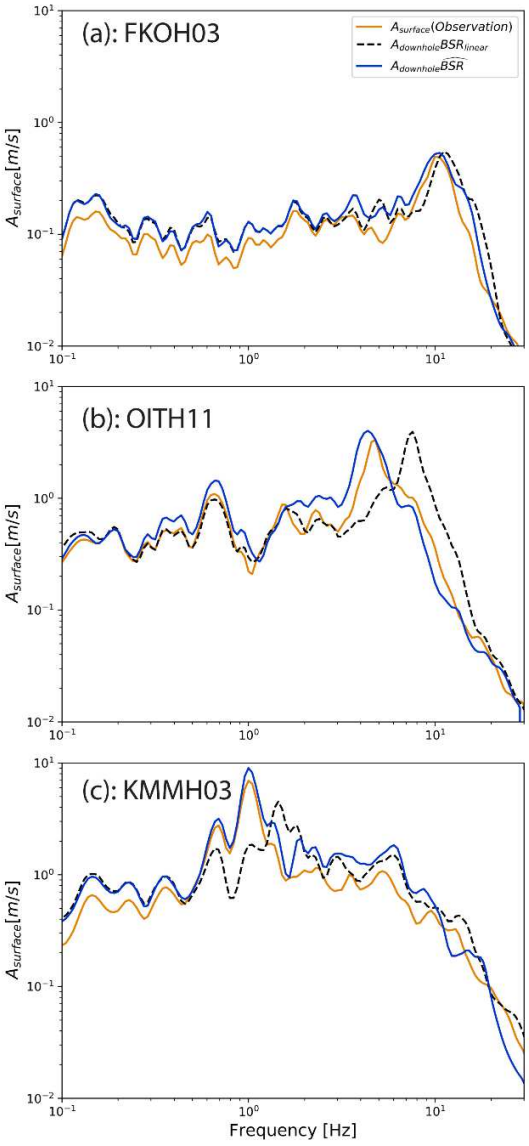

Figure 16. Fourier spectrum at the surface of the horizontal components. Earthquake of Kumamoto 15th April. (a) site FKOH03. (b) site OITH11. (c) site KMMH03. The color version of this figure is available only in the electronic edition.

The predictions of the surface ground motion are improved when the site response is corrected by the adequate frequency shift. Comparing the main peaks frequency position of the Fourier spectra at the surface, Table 4 shows the relative difference between observations and predictions. In the case of the site FKOH03, the difference is small since the target ground motion isn't strong enough to exhibit a non-linear behavior of the soil. But even in this case, the spectra obtained with the *fsp* correction is closer to the observed spectra. For the two other sites, the prediction of the main peak frequency position is improved by more than 40% in both cases in comparison with the direct use of BSR_{linear}.

Table 4. Comparison of the main peaks in the spectra at the surface between the observation and the computed spectra using $\widehat{BSR}$ and BSR_{linear}.

	FKOH03	OITH11	KMMH03
$A_{surface}$ to $\widehat{BSR} \cdot A_{downhole}$	4%	8%	0%
$A_{surface}$ to $BSR_{linear} \cdot A_{downhole}$	10%	60%	44%

5 Discussion

To estimate precisely the ground motion at the surface in the time domain, an inverse Fourier transform should be applied to the estimation of the Fourier spectrum. Additionally, the same previously described process should be applied independently for each horizontal components of then ground motion. However, the phase modification due to the site effects should also be taken into account. This effect has been studied before, and usually, it is assumed that 1D site effect does not modify consequently the phase [40]. Since we are using borehole arrays configuration, the applicability of the same assumptions must be evaluated, and it will be part of future studies.

The application of the parameter *fsp* is very promising for the prediction of the non-linear ground motion. In a simple case, we demonstrate that the parameter *fsp* provides a good evaluation of the shear modulus reduction. In a full non-linear approach, the parameter provides an average quantification of the decrease of the shear modulus. For both cases, the parameter gives a good quantification of the impact of the non-linear soil behavior in the site response.

For now, the definition of the *fsp* parameter requires a vertical array of accelerometers and weak to moderate earthquake recordings to define the *fsp* curves. To overpass this limitation, we are currently working on the prediction of the *fsp* curves at non-instrumented sites but characterized by specific geotechnical parameters as Vs_{30} and f_0 that has been demonstrated to be a good proxy parameter for describing the potential non-linear site behavior of a site (e.g. [10] Régnier et al 2016). To predict the rock motion at the downhole station (with the effects of the down-going waves) several methods could be applied such as the Empirical Green's Function directly at downhole or with a correction method to transfer from surface to borehole as proposed in Cadet et al. [41] or the use of numerical models.

6 Conclusions

We propose in this paper to quantify the effects of non-linear site behavior by measuring the frequency shift that it produces in the Borehole Spectral Ratio (*BSR)* from weak motion to stronger one. The logarithmic shift of *BSR*, that we called frequency shift parameter (*fsp*), is related to the intensity of the ground motion. For each site, we, therefore, defined *fsp* curves that relate the *fsp* parameter to the PGA at the downhole station following the classic hyperbolic model. We thus are able to estimate the non-linear effects of strong ground motions at sites using enough recorded data.

We showed that the frequency shift parameter (*fsp)* is a good proxy for non-linear site behavior, as the *fsp* curves could mimic the shear modulus reduction curves. This fitting is better accomplished when an appropriate parameter to approximate the shear strain in the soil column during the shaking is used.

For the earthquake of Kumamoto 2016, we estimated the non-linear site response and the Fourier spectrum at the surface, including the non-linear effects based on the linear site response and the corresponding rock downhole recording of the earthquake. The prediction provided very close results to the observations and, for sites with high nonlinearity, it improves in our case by more than 40% the frequency position of the main peak compared to a linear evaluation. The *fsp* curves provide, as shear modulus reduction curves do, an evaluation of the propensity of a site to develop non-linearity as well a possible way to quantify the level of non-linearity of the site under strong earthquakes.

Acknowledgments

All authors are thankful with the National Research Institute for Earth Science and Disaster Resilience (NIED) in Japan for making Kik-net data available and collected the used data in this paper. Those data can be obtained from web site www.kyoshin.bosai.go.jp (last accessed October 2017).

We are thankful to the anonymous reviewers for their fruitful comments that improved the manuscript.

Also, we thank the professor Fernando Lopez Caballero from Centrale Supelec, Paris-Saclay France, for his help to interpret the CyberQuake analysis.

The data in this study for any station and ground motion (e.g. *fsp*, *PGA*, *PGV*) are available upon request.

Bibliography

[1] Bard P-Y, Bouchon M. The two-dimensional resonance of sediment-filled valleys. Bull Seismol Soc Am 1985;75:519–41.

[2] Cranswick E, King K, Carver D, Worley D, Williams R, Spudich P, et al. Site response across downtown Santa Cruz, California. Geophys Res Lett 1990;17:1793–6.

[3] Lermo J, Chavez-Garcia FJ. Site effect evaluation using spectral ratios with only one station. Bull Seismol Soc Am 1993;83:1574–94.

[4] Kramer L. Geotechnical earthquake engineering. vol. 1. Prentice-Hall International Series; 1996.

[5] Thompson EM, Baise LG, Kayen RE, Guzina BB. Impediments to Predicting Site Response: Seismic Property Estimation and Modeling Simplifications. Bull Seismol Soc Am 2009;99:2927–49. doi:10.1785/0120080224.

[6] Rubinstein JL. Nonlinear Site Response in Medium Magnitude Earthquakes near Parkfield, CaliforniaNonlinear Site Response in Medium Magnitude Earthquakes near Parkfield, California. Bull Seismol Soc Am 2011;101:275–86. doi:10.1785/0120090396.

[7] Régnier J, Cadet H, Bonilla LF, Bertrand E, Semblat J-F. Assessing Nonlinear Behavior of Soils in Seismic Site Response: Statistical Analysis on KiK-net Strong-Motion Data. Bull Seismol Soc Am 2013;103:1750–70. doi:10.1785/0120120240.

[8] Zeghal M, Elgamal A. Analysis of Site Liquefaction Using Earthquake Records. J Geotech Eng 1994;120:996–1017. doi:10.1061/(ASCE)0733-9410(1994)120:6(996).

[9] Assimaki D, Li W, Steidl J, Schmedes J. Quantifying Nonlinearity Susceptibility via Site-Response Modeling Uncertainty at Three Sites in the Los Angeles Basin. Bull Seismol Soc Am 2008;98:2364–90. doi:10.1785/0120080031.

[10] Régnier J, Cadet H, Bard P-Y. Empirical Quantification of the Impact of Nonlinear Soil Behavior on Site Response. Bull Seismol Soc Am 2016;106:1710–9.

[11] Bonilla LF, Archuleta RJ, Lavallée D. Hysteretic and Dilatant Behavior of Cohesionless Soils and Their Effects on Nonlinear Site Response: Field Data Observations and Modeling. Bull Seismol Soc Am 2005;95:2373–95. doi:10.1785/0120040128.

[12] Pavlenko OV. Possible Mechanisms for Generation of Anomalously High PGA During the 2011 Tohoku Earthquake. Pure Appl Geophys 2017;174:2909–24. doi:10.1007/s00024-017-1558-2.
[13] Aguirre J, Irikura K. Nonlinearity, liquefaction, and velocity variation of soft soil layers in Port Island, Kobe, during the Hyogo-ken Nanbu earthquake. Bull Seismol Soc Am 1997;87:1244–58.
[14] Iai S, Morita T, Kameoka T, Matsunaga Y, Abiko K. Response of a Dense Sand Deposit during 1993 Kushiro-Oki Earthquake. Soils Found 1995;35:115–31. doi:10.3208/sandf1972.35.115.
[15] Wen K-L. Non-linear soil response in ground motions. Earthq Eng Struct Dyn 1994;23:599–608. doi:10.1002/eqe.4290230603.
[16] Ishibashi I, Zhang X. Unified dynamic shear moduli and damping ratios of sand and clay. SOILS Found 1993;33:182–91. doi:10.3208/sandf1972.33.182.
[17] Vucetic Mladen. Cyclic Threshold Shear Strains in Soils. J Geotech Eng 1994;120:2208–28. doi:10.1061/(ASCE)0733-9410(1994)120:12(2208).
[18] Zeghal M, Elgamal AW, Tang HT. Lotung Downhole Array. II: Evaluation of Soil Nonlinear Properties | Journal of Geotechnical Engineering | Vol 121, No 4. J Geotech Eng 1995;121. doi:10.1061/(ASCE)0733-9410(1995)121:4(363).
[19] Glaser S, Baise L. System identification estimation of soil properties at the Lotung site - ScienceDirect. Soil Dyn Earthq Eng 2000;19:521–31. doi:10.1016/S0267-7261(00)00026-9.
[20] Pavlenko OV, Irikura K. Estimation of Nonlinear Time-dependent Soil Behavior in Strong Ground Motion Based on Vertical Array Data. Pure Appl Geophys 2003;160:2365–79. doi:10.1007/s00024-003-2398-9.
[21] Nakata N, Snieder R. Estimating near-surface shear wave velocities in Japan by applying seismic interferometry to KiK-net data. J Geophys Res Solid Earth 2012;117. doi:10.1029/2011JB008595.
[22] Bonilla LF, Guéguen P, Lopez-Caballero F, Mercerat ED, Gélis C. Prediction of non-linear site response using downhole array data and numerical modeling: The Belleplaine (Guadeloupe) case study. Phys Chem Earth Parts ABC 2017;98:107–18. doi:10.1016/j.pce.2017.02.017.
[23] Noguchi S, Sasatani T. Quantification of degree of nonlinear site response, 2008, p. 0049.
[24] Lussou P, Bard P-Y, Modaressi H, Gariel J-C. Quantification of soil non-linearity based on simulation. Soil Dyn Earthq Eng 2000;20:509–16. doi:10.1016/S0267-7261(00)00100-7.
[25] Field EH, Johnson PA, Beresnev IA, Zeng Y. Nonlinear ground-motion amplification by sediments during the 1994 Northridge earthquake. Nature 1997;390:599–602. doi:10.1038/37586.
[26] Boore DM. On Pads and Filters: Processing Strong-Motion Data. Bull Seismol Soc Am 2005;95:745–50. doi:10.1785/0120040160.
[27] Oppenheim AV, Schafer RW. Discrete-time signal processing. Pearson Higher Education; 2010.
[28] Konno K, Ohmachi T. Ground-motion characteristics estimated from spectral ratio between horizontal and vertical components of microtremor. Bull Seismol Soc Am 1998;88:228–41.
[29] Field EH, Jacob KH. A comparison and test of various site-response estimation techniques, including three that are not reference-site dependent. Bull Seismol Soc Am 1995;85:1127–43.
[30] Régnier J, Bonilla L-F, Bard P-Y, Bertrand E, Hollender F, Kawase H, et al. PRENOLIN: International Benchmark on 1D Nonlinear Site-Response Analysis—Validation Phase Exercise. Bull Seismol Soc Am 2018.
[31] Duncan J, Chang C. Nonlinear analysis of stress and strain in soils. ASCE J Soil Mech Found 1970;96:1629–53.
[32] Ishihara K. Soil Behaviour in Earthquake Geotechnics. Oxford: Clarenton Press; 1996.
[33] Chandra J, Guéguen P, Bonilla LF. PGA-PGV/Vs considered as a stress–strain proxy for predicting nonlinear soil response. Soil Dyn Earthq Eng 2016;85:146–60. doi:10.1016/j.soildyn.2016.03.020.
[34] Modaressi H, Foerster E. CyberQuake. User's Man BRGM Fr 2000.
[35] Hujeux J. Une loi de comportement pour le chargement cyclique des sols. Génie Parasismique 1985:287–302.
[36] Lopez-Caballero F, Modaressi-Farahmand-Razavi A, Modaressi H. Nonlinear numerical method for earthquake site response analysis I — elastoplastic cyclic model and parameter identification strategy. Bull Earthq Eng 2007;5:303–23. doi:10.1007/s10518-007-9032-7.
[37] Kaklamanos J, Bradley BA, Thompson EM, Baise LG. Critical Parameters Affecting Bias and Variability in Site-Response Analyses Using KiK-net Downhole Array DataCritical Parameters Affecting Bias and

562 Variability in Site-Response Analyses. Bull Seismol Soc Am 2013;103:1733–49.
563 doi:10.1785/0120120166.
564 [38] Asano K, Iwata T. Source rupture processes of the foreshock and mainshock in the 2016 Kumamoto
565 earthquake sequence estimated from the kinematic waveform inversion of strong motion data. Earth
566 Planets Space 2016;68:147. doi:10.1186/s40623-016-0519-9.
567 [39] Yagi Y, Okuwaki R, Enescu B, Kasahara A, Miyakawa A, Otsubo M. Rupture process of the 2016
568 Kumamoto earthquake in relation to the thermal structure around Aso volcano. Earth Planets Space
569 2016;68:118. doi:10.1186/s40623-016-0492-3.
570 [40] Fleur SS, Bertrand E, Courboulex F, Lépinay BM de, Deschamps A, Hough S, et al. Site Effects in Port-au-
571 Prince (Haiti) from the Analysis of Spectral Ratio and Numerical Simulations. Bull Seismol Soc Am 2016.
572 doi:10.1785/0120150238.
573 [41] Cadet H, Bard P-Y, Rodriguez-Marek A. Site effect assessment using KiK-net data: Part 1. A simple
574 correction procedure for surface/downhole spectral ratios. Bull Earthq Eng 2012;10:421–48.
575 doi:10.1007/s10518-011-9283-1.
576